NeuroImage: Clinical 42 (2024) 103616

Contents lists available at ScienceDirect

NeuroImage: Clinical

journal homepage: www.elsevier.com/locate/ynicl

Full kinetic modeling analysis of [^{18}F]fluorocholine Positron Emission Tomography (PET) at initial diagnosis of high-grade glioma

Sebastià Rubí [a,b,c,*], Pedro Bibiloni [c,d], Marina Villar [a], Marta Brell [b,c,e], Manuel Valiente [a], Margalida Galmés [f], María Toscano [a], Gabriel Matheu [c,g], José Luis Chinchilla [a], Jesús Molina [a], José Luis Valera [c,h], Ángel Ríos [c], Meritxell López [c], Cristina Peña [a,c]

[a] Department of Nuclear Medicine, Hospital Universitari Son Espases, 07010 Palma, Spain
[b] Department of Medicine, University of the Balearic Islands, E-07122 Palma, Spain
[c] Health Research Institute of the Balearic Islands (IdISBa), 07010 Palma, Spain
[d] SCOPIA Research Group, University of the Balearic Islands, E-07122 Palma, Spain
[e] Department of Neurosurgery, Hospital Universitari Son Espases, 07010 Palma, Spain
[f] Department of Nuclear Medicine, Hospital Quironsalud Palmaplanas, 07010 Palma, Spain
[g] Department of Pathology, Hospital Universitari Son Espases, 07010 Palma, Spain
[h] Department of Pulmonology, Hospital Universitari Son Espases, 07010 Palma, Spain

ARTICLE INFO

Keywords:
Kinetic modeling
PET
[^{18}F]fluoromethylcholine
High-grade glioma

ABSTRACT

Purpose: The main objective was to characterize the tracer uptake kinetics of [^{18}F]fluoromethylcholine ([^{18}F]F-CHO) in high-grade gliomas (HGG) through a full PET kinetic modeling approach. Secondarily, we aimed to explore the relationship between the PET uptake measures and the HGG molecular features.

Materials and methods: Twenty-four patients with a suspected diagnosis of HGG were prospectively included. They underwent a dynamic brain [^{18}F]F-CHO-PET/CT, from which a tumoral time-activity curve was extracted. The plasma input function was obtained through arterial blood sampling with metabolite correction. These data were fitted to 1- and 2-tissue-compartment models, the best of which was selected through the Akaike information criterion. We assessed the correlation between the kinetic parameters and the conventional static PET metrics (SUV_{max}, SUV_{mean} and tumor-to-background ratio TBR). We explored the association between the [^{18}F]F-CHO-PET quantitative parameters and relevant molecular biomarkers in HGG.

Results: Tumoral time-activity curves in all patients showed a rapid rise of [^{18}F]F-CHO uptake followed by a plateau-like shape. Best fits were obtained with near-irreversible 2-tissue-compartment models. The perfusion-transport constant K_1 and the net influx rate K_i showed strong correlation with SUV_{max} ($r = 0.808–0.861$), SUV_{mean} ($r = 0.794–0.851$) and TBR ($r = 0.643–0.784$), $p < 0.002$. HGG was confirmed in 21 patients, of which those with methylation of the O-6-methylguanine-DNA methyltransferase (MGMT) gene promoter showed higher mean K_i ($p = 0.020$), K_1 ($p = 0.025$) and TBR ($p = 0.001$) than the unmethylated ones.

Conclusion: [^{18}F]F-CHO uptake kinetics in HGG is best explained by a 2-tissue-compartment model. The conventional static [^{18}F]F-CHO-PET measures have been validated against the perfusion-transport constant (K_1) and the net influx rate (K_i) derived from kinetic modeling. A relationship between [^{18}F]F-CHO uptake rate and MGMT methylation is suggested but needs further confirmation.

1. Introduction

High-grade gliomas (HGG) are the most common primary brain tumors in adults and are a high-mortality disease that remains a treatment challenge. They are classified as grade 3 and grade 4 gliomas in the World Health Organization Classification of Central Nervous System tumors (CNS WHO Classification) (Louis et al., 2021). The use of Positron Emission Tomography (PET) neuroimaging biomarkers in these tumors has gained interest in several clinical settings (Law et al., 2019; Albert et al., 2024), including that of the treatment-naive HGGs in which the non-invasive inference of prognostic and predictive information can be of utility as a surrogate of their pathological and molecular

* Corresponding author at: Department of Nuclear Medicine, Hospital Universitari Son Espases, Carretera Valldemossa 79, 07010 Palma, Spain.
E-mail address: sebastia.rubi@ssib.es (S. Rubí).

https://doi.org/10.1016/j.nicl.2024.103616
Received 27 September 2023; Received in revised form 25 April 2024; Accepted 5 May 2024
Available online 6 May 2024

alterations.

Amino acid analogues are the first-line PET radiopharmaceuticals in neuro-oncology. Nevertheless, the fluorinated tracers [^{18}F]fluoro-ethyl-tyrosine and [^{18}F]fluorodopa are still not widely available in all countries, while the clinical use of [^{11}C]methionine is limited by its short half-life requiring an on-site cyclotron facility. Thus, it is still interesting to explore the biological and clinical behavior of alternative radiopharmaceuticals with high lesion-to-background performance in the CNS. Radiolabeled choline analogues, which are markers of lipogenesis and synthesis of cell membrane, meet this requirement and have the advantage to be a widely available and well-known radiopharmaceuticals with an extensive use in other clinical indications. The fluorinated analogue [^{18}F]fluoromethylcholine ([^{18}F]F-CHO) has a rapid blood clearance, a virtually absent uptake in normal brain tissue and an increased retention in high grade gliomas (DeGrado et al., 2001; Kwee et al., 2007). This has been mainly assessed through visual inspection and PET metrics based on standardized uptake value (SUV), tumor-to-background ratio (TBR) and other static quantitative features (Sollini et al., 2018; García Vicente et al., 2019; Kong et al., 2021; Kong et al., 2021). Nevertheless, in Nuclear Medicine, the static uptake measures of a PET radiopharmaceutical for a specific clinical application must ideally be validated against a kinetic modeling analysis to ensure that their values have some kind of proportionality with the several absolute uptake rate constants involved in their tissue biodistribution (Pantel et al., 2022). Despite this practice is strongly encouraged amongst the scientific PET community (Lammertsma, 2017), it has not yet been reported for [^{18}F]F-CHO in human gliomas. Specifically, there are limited data available on how the [^{18}F]F-CHO transport through the damaged blood–brain barrier (BBB) and specific membrane transporters, on the one hand, and enzymatic intracellular phosphorylation, on the other, differentially contribute to the static PET signal of these tumors. (Cuccurullo et al., 2017). Moreover, choline and its radiolabeled analogues undergo an important oxidative metabolism that is catalyzed by choline-oxidase, an enzyme that is present in various tissues and gives rise to its main plasmatic metabolite, [^{18}F]fluorobetaine (Roivainen et al., 2000; Slaets and De Vos, 2013).

Based on this rationale, our primary aim was to determine the appropriate compartment model for [^{18}F]F-CHO in HGGs through a standard full kinetic modeling methodology, including the acquisition of dynamic PET data, an arterial plasma input function and a chromatography-based metabolite correction. Subsequently, we aimed to validate the use of routine static [^{18}F]F-CHO-PET measures against the kinetic rate constants derived from the compartmental analysis. Finally, as a secondary objective, we explored whether the [^{18}F]F-CHO uptake parameters could have additional value in the prediction of the molecular characteristics of these tumors.

2. Material and methods

2.1. Patients

Twenty-four patients (13 males, 11 females; 29–81 years, median age 54) were prospectively included (Fig. 1) from July 2016 to January 2020 in the Son Espases University Hospital (Palma, Spain). We included adult patients (>18 years old) with a newly diagnosed brain lesion suggestive of HGG by magnetic resonance imaging (MRI) which was suitable for complete surgical resection. Patients with a previous diagnosis of low-grade glioma or with previous brain surgical procedures and/or other causes of brain anatomical distortion that were not related to the recently diagnosed lesion were excluded from the study. The study was approved by the local ethics committee (CEI-IB: Research Ethics Committee of the Balearic Islands, Protocol IB 3067/15 PI), and all patients provided written informed consent after receiving verbal and written explanation regarding the examination and use of their anonymized data for research and publication purposes.

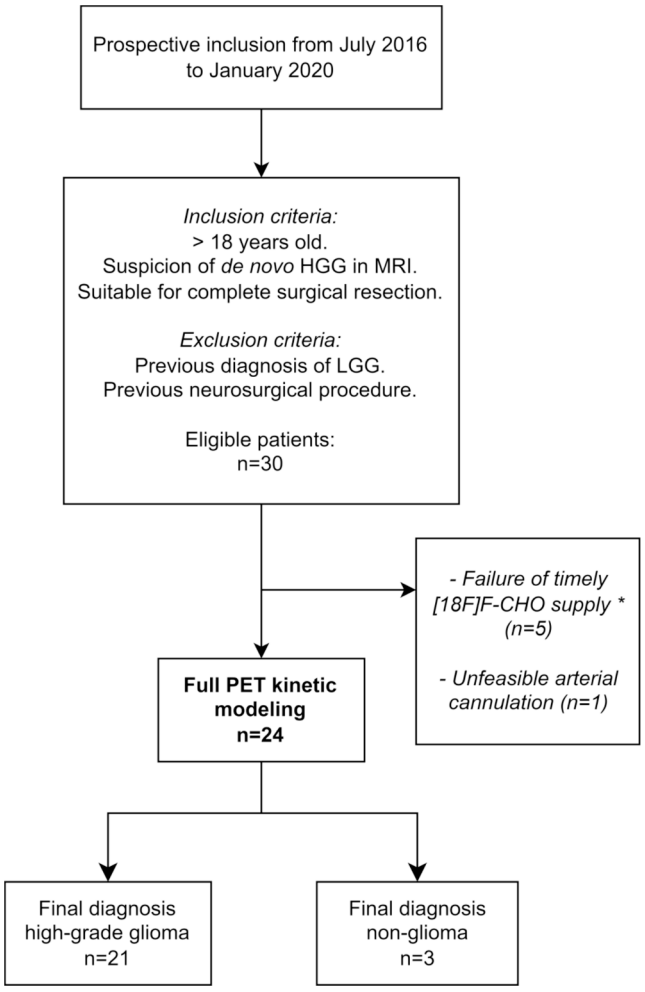

Fig. 1. Flowchart of the study. Between 2016 and 2020, we included adult patients (>18 years old) with a newly diagnosed brain lesion suggestive of HGG by magnetic resonance imaging (MRI) which was suitable for complete surgical resection. Patients with a previous diagnosis of low-grade glioma or with previous brain surgical procedures and/or other causes of brain anatomical distortion that were not related to the recently diagnosed lesion were excluded from the study. MRI: magnetic resonance imaging with common sequences (including gadolinium intravenous injection) and advanced techniques. HGG: high-grade glioma. LGG: low-grade glioma. *PET scan was usually scheduled a few days before surgery.

2.2. PET/CT imaging

Each patient underwent a 45 min dynamic brain PET scan on a GE Discovery PET/CT 600 (GE Healthcare, Inc.) immediately after a slow bolus injection of 5 MBq/kg (0.14 mCi/kg) of [^{18}F]F-CHO. Images were reconstructed into 36 frames (10 × 5 s, 4 × 10 s, 3 × 20 s, 5 × 30 s, 5 × 60 s, 4 × 150 s, 5 × 300 s). Additionally, a static PET volume was reconstructed from 20 min to 45 min post-injection to calculate standard routine uptake measures.

2.3. Arterial blood sampling and metabolite analysis

Twenty-seven consecutive blood samples from a catheter placed in the radial artery were manually obtained over a period of 40 min, from the start of PET acquisition: 10 × 5 s, 3 × 10 s, 3 × 15 s, 6 × 60 s, 2 × 180 s, 1 × 300 s, and 2 × 600 s. Each sample was measured in a calibrated well counter (2480 WIZARD2 Gamma Counter, Perkin Elmer, Inc), and the decay-corrected activity concentration in whole blood and plasma was obtained in kBq/ml.

Since this arterial input function must only represent the radioactivity (kBq/ml) bound to the injected radiopharmaceutical, and not that which is associated to its plasma metabolites, it is necessary to estimate the [^{18}F]F-CHO fraction (or parent fraction) of this activity at any given moment. Thus, five of the arterial samples were deproteinized and developed by thin layer chromatography (TLC) to obtain a parent fraction curve for each patient, following a procedure already described by our group (Villar et al., 2019) to separate [^{18}F]F-CHO from its main plasma metabolite, [^{18}F]fluorobetaine.

2.4. Kinetic analysis

2.4.1. Full-kinetic modeling

The image processing and kinetic modeling was performed in PMOD v3.9 (PMOD Technologies, Ltd).

The metabolite-corrected input function for each patient was obtained from multiplying the arterial plasma time-activity curve (TAC) to the monoexponential fitted parent fraction curve (Villar et al., 2019).

A volume of interest (VOI) encompassing the 100 hottest connected voxels (0.45 cm^3) on the averaged PET image was applied to the whole set of PET dynamic frames to derive the tumoral TAC for each patient.

Several compartment models were fitted to the tumoral TACs. In these models, tracer kinetics is separated into tissue compartments that are connected to each other and to the arterial plasma compartment by transport rate constants. The plasma compartment is represented by the aforementioned arterial input function. First of all, we evaluated the reversible and irreversible 2-tissue-compartment models, with four and three constants, respectively (2T4k and 2T3k), and with intratumoral blood volume fraction (v_B) as an additional fitting parameter (Fig. 2). In these models, K_1 (ml/min/cm^3) theoretically accounts for the transport of the [^{18}F]F-CHO across the BBB and across the choline transporter at the cell membrane of the tumoral cells, k_2 (min^{-1}) is the washout constant from tissue to plasma, k_3 (min^{-1}) represents the rate at which [^{18}F]F-CHO is phosphorylated, and k_4, when non-negligible, is the [^{18}F]F-CHO dephosphorylation rate. Since a trapping mechanism for [^{11}C]choline has already been suggested in gliomas by means of Patlak plot (Patlak et al., 1983), we also applied this graphical analysis to our data with [^{18}F]F-CHO. The Patlak plot after an equilibration time should fit a straight line whose slope equals the net influx rate to the last compartment (Ki^P). The Ki^P was then compared to the influx rate K_i calculated from the full kinetic analysis of 2-tissue-compartment models as $K_i = K_1 \cdot k_3 / (k_2 + k_3)$. Lastly, the simpler 1-tissue-compartment model with two rate constants (1T2k) was also evaluated and compared to the 2-tissue models (Fig. 2). The best model was selected on the basis of the Akaike information criterion (AIC).

Given the concern about a possible significant nonspecific uptake of the main plasmatic radiometabolite ([^{18}F]fluorobetaine) into the tumoral lesion, a 3-tissue-compartment model with two input functions (3T2i) was tested and compared with the previously selected model. A diagram and more details of this model are provided in Supplemental Fig. 1.

To obtain distribution statistics of the parameter estimates in the selected models, we conducted a Markov chain Monte Carlo (MCMC) simulation (Hines et al., 2014) by considering a Random Walk Metropolis algorithm, which was implemented in MATLAB version R2022a (The MathWorks Inc., Natick, MA, USA). The range between the 5th and the 95th percentiles of the random walk parameter distribution was divided by its mid-value to obtain a normalized plausible range for each parameter as a measure of its identifiability. The MATLAB code implementing the MCMC simulation is made fully available upon direct request to the corresponding author.

More details on the methods described so far are available as Supplemental Material.

2.4.2. Kinetic parameters versus routine clinical measures, VOI-based and voxel-wise

We assessed the correlations of the main kinetic rate constants with the mean and maximum standardized uptake values (SUV_{mean} and SUV_{max}) and tumor-to-background ratio (TBR = SUV_{max} / contralateral symmetric SUV_{mean}) extracted from a static PET volume (20–45 min post-injection). To perform a voxel-wise correlation analysis, we generated tumoral parametric maps for each patient, which were compared to the corresponding SUV images on a voxel-by-voxel basis.

2.5. Histopathological and molecular analysis

Preoperative MRI and PET SUV image coregistration was performed in all cases, in order to better guide tumor resection. Tumor areas with the highest [^{18}F]F-CHO uptake were specifically identified with intraoperative neuronavigation, resected and properly labeled for the pathologist. Each tumor was categorized according to the CNS WHO Classification. For glial tumors, the molecular analysis was focused on isocitrate dehydrogenase (IDH) mutational status and O-6-Methylguanine-DNA methyltransferase (MGMT) gene promoter methylation. The former is key in the WHO classification of adult-type diffuse gliomas and the latter is an epigenetic marker of high relevance in HGG, as a

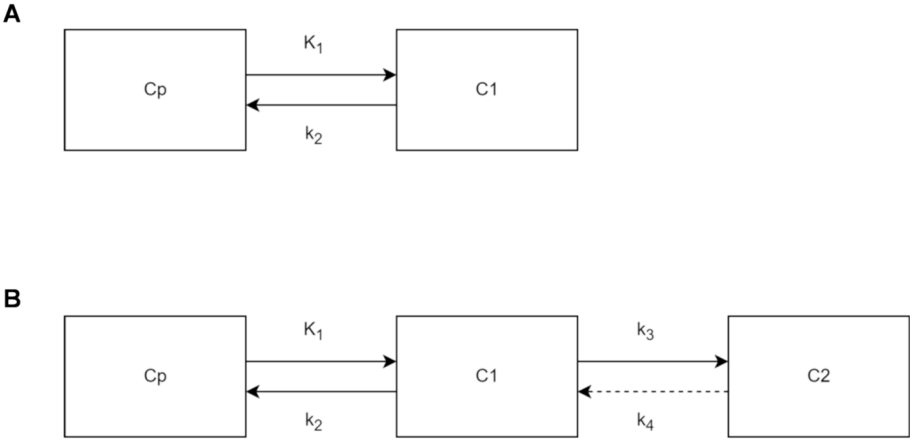

Fig. 2. Diagrams of (A) 1-tissue compartment model with two rate constants (1T2k) and (B) 2-tissue compartment model with k_4 (2T4k) and without k_4 (2T3k). See a detailed description in section 2.4.1. of the main text. C1: free non-metabolized tracer; C2: intracellular metabolized tracer, with (if $k_4 = 0$) or without trapping; C_p: plasma activity concentration. Intratumoral blood volume fraction (v_B) was also included as a fitting parameter in all models. The operational equation which models the PET tumoral time-activity curve in the 2-tissue compartment model is $C_{model} = (1 - v_B)\cdot(C_1(t) + C_2(t)) + v_B \cdot C_{wb}(t)$, where C_{wb} stands for the whole blood activity concentration.

methylated MGMT promoter has been associated with a better response to alkylating agents and a longer survival (Butler et al., 2020). The IDH mutational status was determined by immunohistochemistry with anti-IDH1 R132H antibody H09 (BenchMark Ultra immunostainer, Ventana Medical Systems, Tucson, AZ, USA). The MGMT gene promoter methylation was assessed by pyrosequencing (Therascreen MGMT Pyro Kit, PyroMark Q24 pyrosequencer, Qiagen, Hilden, Germany). Three categories were established based on the average level of percentage methylation in four CpG sites located in exon 1 of the MGMT gene: non-methylation (<9%), intermediate methylation (9–29 %) and high methylation (>29 %) (Gurrieri et al., 2018).

2.6. Statistical analysis

Median and interquartile range (IQR) were used to describe quantitative variables.

For comparison of quantitative variables related to the kinetic modeling analysis, we used parametric (Student's t) or non-parametric (Wilcoxon signed-rank) statistical tests for paired groups, depending on normality of the data distributions, as well as the Pearson's *r* correlation coefficient and intraclass correlation coefficients (ICC_{cons} for consistency and ICC_{abs} for absolute agreement) (Shrout and Fleiss, 1979).

The relationship between the status of the above mentioned molecular biomarkers and the quantitative PET measures was assessed through the non-parametric Mann-Whitney *U* test, as well as a receiver operating characteristic (ROC) curve analysis when a statistically significant relationship was detected.

Statistical analysis was performed using IBM SPSS Statistics version 22.0 (IBM Corp, Armonk, NY, USA). A p-value of < 0.05 was considered as statistically significant.

The data used in the study can be made available upon request to the corresponding author and is subject to the approval by the local ethics committee (CEI-IB).

3. Results

In the 24 patients, MRI revealed supratentorial masses with intense gadolinium contrast enhancement in 23 of them. The static reconstructed PET images showed much higher [^{18}F]F-CHO uptake in the tumors compared to the normal brain tissue in those 23 patients. One patient showed very mild gadolinium enhancement, along with the lowest tumoral [^{18}F]F-CHO uptake in our cohort (patient 20, see the Table in Supplemental Material). Visually, the coregistered PET/MRI fusion images revealed that the uptake of [^{18}F]F-CHO was roughly spatially concordant with the gadolinium-enhancing volume on MRI in all patients. Minor mismatches between gadolinium and [^{18}F]F-CHO patterns were observed in eight patients. The most active voxels in the PET image were always located within a gadolinium-enhancing portion of the tumor.

The plasma and whole blood TACs of the 24 analyzed patients, as well as their metabolite corrected arterial input functions, showed a fast initial peak with a rapid decline. At 10 min post-injection, the activity concentration in whole blood was < 7 % of the initial peak in all patients.

The parent fraction values of [^{18}F]F-CHO in arterial plasma for the 24 analyzed patients yielded by the TLC analysis were (expressed as median (IQR)): 95.6 % (4.9 %), 68.3 % (19.2 %), 48.9 % (20.9 %), 44.3 % (16.9 %), 37.8 % (12.7 %) and 34.5 % (8.1 %) at average sampling times of 3, 6, 9, 12, 15 and 20 min, respectively (Fig. 3).

Tumoral TACs in all patients showed a rapid rise of intratumor [^{18}F]F-CHO uptake followed by a plateau-like shape (Fig. 3). A slow rising slope was observed in a few cases. In 11 out of 24 patients, the plateau-like phase was preceded by an initial vascular peak (see Fig. 4).

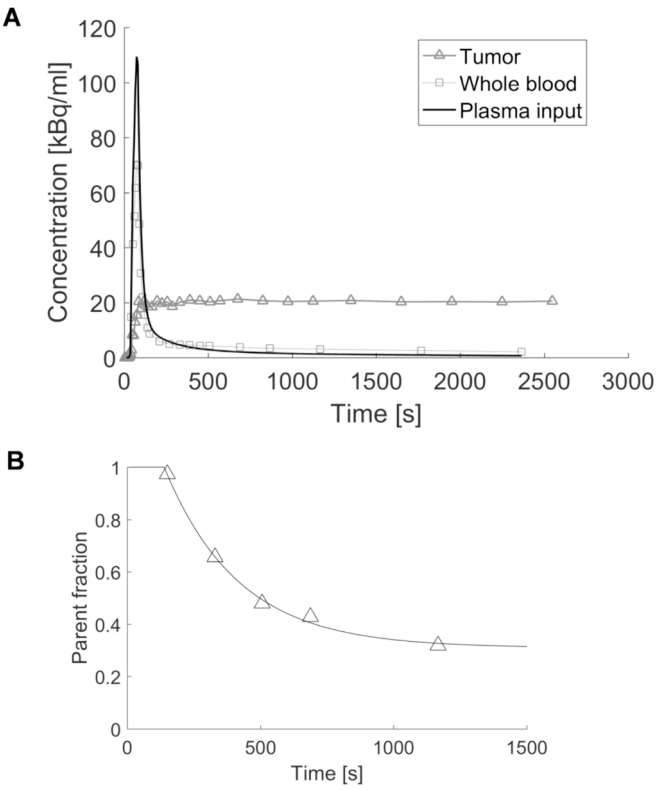

Fig. 3. (A) Time activity curves (TAC) of a 53-year-old man with glioblastoma, IDH wildtype: experimental TACs (with linear interpolation) for arterial whole-blood and tumoral PET uptake are shown, as well as the triexponential model fitting for the metabolite-corrected plasma input function. (B) Parent fraction curve of the same patient (experimental points and monoexponential fitting; note that negligible metabolites are assumed before a *begin time*), which was used for the metabolite correction.

3.1. Full-kinetic modeling and parameter identifiability

The median (IQR) of the AIC values from the 24 cases was significantly lower for the 2-tissue models compared to those of the 1-tissue model ($p < 0.001$): 327.5 (30.2) and 334.5 (28.5) for the 2T4k + v_B and 2T3k + v_B models, respectively, and 351.8 (43.6) for the 1T2k + v_B model. Individually considered, 23 out of 24 cases showed lower AIC values for the 2-tissue models. The curve fitting of the 1T2k + v_B model was visually poor in the vast majority of patients (Fig. 4). No significant differences were seen among the AIC values of 2T4k + v_B and 2T3k + v_B models ($p = 0.065$). Individually considered, 16 out of 24 patients showed lower AIC values for the reversible 2T4k + vB model, which also displayed a better visual curve fitting. Nevertheless, the k_4 values in these patients were consistently small, with a median (IQR) of 0.023 (0.010). The Patlak plot showed a good linear fit in all patients (median $R^2 = 0.99$) and the slope Ki^P showed a good consistency ($ICC_{cons} = 0.853$) and absolute agreement ($ICC_{abs} = 0.762$) with the K_i values from the full-kinetic modeling ($p < 0.001$). For all the above reasons, we accepted the hypothesis of two compartments in the tumoral tissue with an irreversible ($k_4 = 0$, in 8 patients) or near-irreversible trapping (small k_4, in 16 patients) in the last compartment.

The results of the comparison of the selected 2-tissue models with the more complex 3-tissue model with tumoral metabolite input are available as Supplemental Material (Supplemental Fig. 2). Briefly, the AIC values for both type of models did not show statistical differences ($p = 0.78$), and their main kinetic parameters showed a moderate to good agreement.

The values of the 2-tissue model parameter estimates and their distribution statistics from the MCMC simulations are summarized in

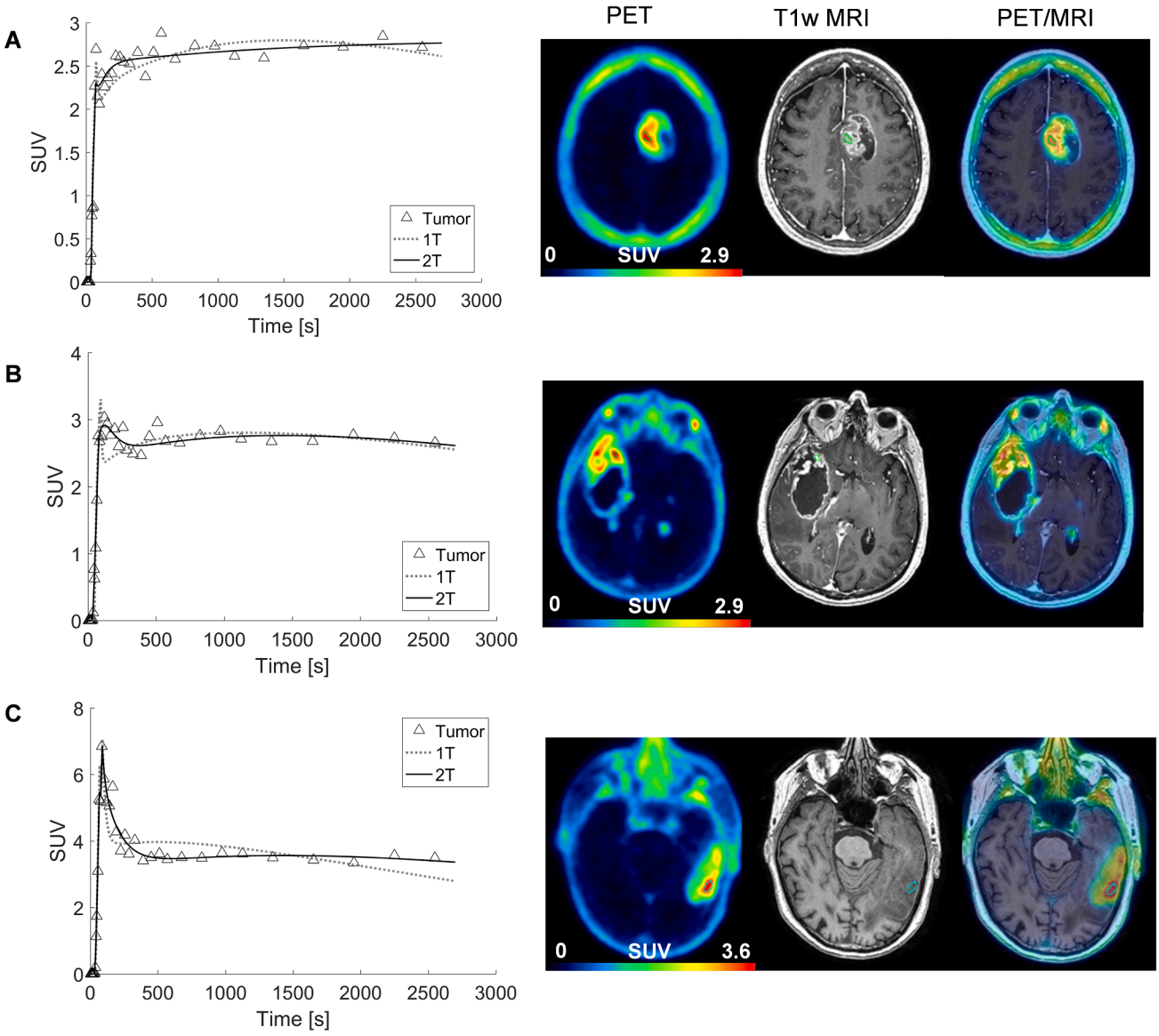

Fig. 4. Kinetic modeling of representative [^{18}F]F-CHO time-activity patterns in three patients with glioblastoma, IDH wildtype, with their corresponding static images. (A) 51-year-old female; (B) 67-year-old male; (C) 75-year-old male. Tumoral PET time-activity curves (triangles) and their fitting to a 1-tissue (1T) and 2-tissue (2T) compartment models are shown. The case depicted in C was the only patient in which gadolinium injection in the T1w MRI was not advised, due to chronic renal failure.

Table 1. According to their normalized plausible ranges (>100 %), k_2 and k_3 were not considered identifiable as individual parameters. That is, a wide range of different combinations of values for these parameters could explain the tumoral curve equally well. Therefore, both were excluded from further analysis.

3.2. Uptake kinetic parameters versus routine clinical measures

Both K_1 and K_i for the selected 2-tissue models in the 24 patients showed a good positive linear correlation with the SUV_{max} ($r = 0.808$ for K_1 and 0.861 for K_i, $p < 0.001$) and the SUV_{mean} ($r = 0.794$ for K_1 and 0.851 for K_i, $p < 0.001$). For the TBR index, the degree of correlation was slightly lower ($r = 0.643$ for K_1 and 0.784 for K_i, $p < 0.002$) (Figs. 5 and 6).

We obtained parametric images of Patlak slope K_i^P inside the whole tumoral region, which showed an excellent voxel-wise correlation with the SUV image in each of the 24 patients (Supplemental Fig. 3), with a median correlation coefficient $r = 0.976$ (IQR 0.054).

3.3. Relationship between quantitative PET parameters and molecular features in high-grade gliomas

The demographic features and postsurgical histopathological findings of the 24 patients are summarized in Table 2 (21 HGGs and three non-gliomas). See also the extended Table in the Supplemental Material for details of each individual patient.

As seen in Table 2, all but one of the patients with HGG were classified as glioblastoma IDH wildtype (CNS WHO grade 4). The MGMT promoter was unmethylated in 14 out of the 21 patients with HGG, and it showed some degree of methylation in the remaining seven. Thus, we assessed the relationship between the MGMT methylation status and [^{18}F]F-CHO uptake parameters, including the identifiable [^{18}F]F-CHO kinetic rate constants K_1 and K_i, as well as the traditional static SUV-based measures. The group of patients with methylated tumors

Table 1
Descriptive statistics of the 2-tissue model parameter estimates in the 24 patients, along with their distribution statistics derived from the Markov chain Monte Carlo (MCMC) simulation.

Parameter	Median (IQR)	MCMC simulation	
		Plausible range* (median)	**Normalized plausible range†** (median)
K_1 (ml/min/cm^3)	0.132 (0.085)	0.014	9.8 %
k_2 (min^{-1})	0.103 (0.151)	0.110	114.5 %
k_3 (min^{-1})	0.176 (0.147)	0.392	142.13 %
K_i (ml/min/cm^3)	0.079 (0.040)	0.017	23.4 %
v_B	0.077 (0.032)	0.012	19.1 %

* Calculated as the 95th percentile minus the 5th percentile of the random walk parameter distribution. †Calculated as the plausible range divided by its mid-value. IQR = interquartile range; v_B = blood volume fraction.

showed higher kinetic uptake values than the unmethylated group with statistical significance ($p = 0.020$ for K_i and $p = 0.025$ for K_1). Among the static measures, TBR showed a significant relationship ($p = 0.001$) with MGMT methylation, while SUV_{max} and SUV_{mean} achieved a borderline significance ($p = 0.046$). Boxplots for K_1, K_i and TBR are depicted in Fig. 7. The ROC analysis results are summarized in Table 3. ROC curves are available in Supplemental Fig. 4.

4. Discussion

Our study addresses for the first time the absolute uptake quantification of the fluorinated analogue [^{18}F]F-CHO in human gliomas through a full kinetic modeling approach, including arterial blood sampling and experimental metabolite correction in each individual patient. It validates the use of simplified uptake PET metrics as surrogates of the absolute kinetic quantification parameters. So far, the PET kinetic modeling of radiolabeled choline analogues in human neoplasms has only been addressed in about ten studies and, to the best of our knowledge, only two of them have dealt with brain tumors (Utriainen et al., 2003; Grkovski et al., 2020). These studies have been conducted with a somehow simplified kinetic modeling procedure. The study of Utriainen et al. (Utriainen et al., 2003) with [^{11}C]choline included a heterogeneous cohort of 12 brain tumors and was limited to Patlak graphical analysis, while Grkovski et al. (Grkovski et al., 2020), in their cohort of 14 patients with brain metastases with [^{18}F]F-CHO, used an image derived input function as an alternative to arterial sampling and an external population-based parent fraction curve instead of direct metabolite analysis. As previously shown by our group (Villar et al., 2019), small amounts of radioactivity are slowly accumulating in red blood cells after the [^{18}F]F-CHO intravenous injection. Thus, for the blood-derived time-activity curves to adequately represent the [^{18}F]F-CHO available to the target tissue, i.e. the input function, blood centrifugation and direct plasmatic counting were performed for each sample in our study, in addition to whole-blood measures. Moreover, the input function needs to account for the systemic oxidation of [^{18}F]F-CHO to [^{18}F]fluorobetaine. The time-dependent fractions of

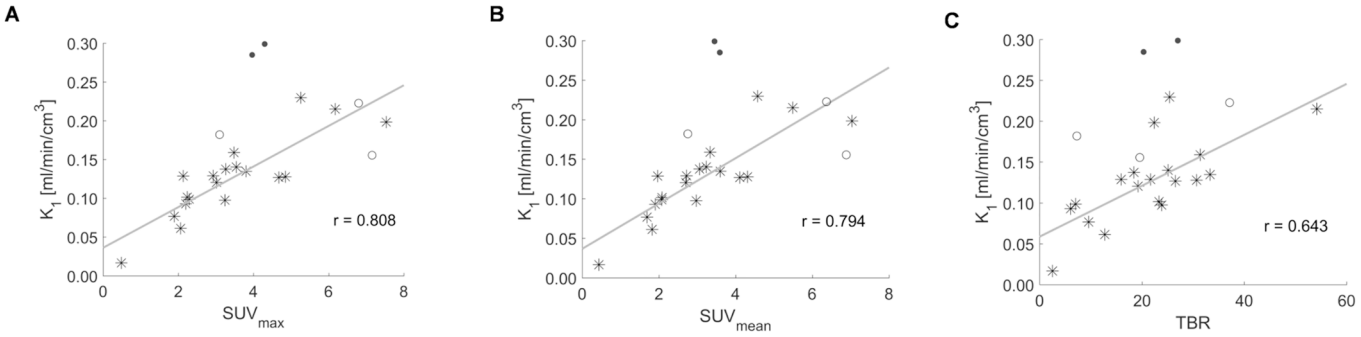

Fig. 5. Correlation between the K_1 rate constant and clinical routine measures in the 24 analyzed patients: SUV_{max} (A), SUV_{mean} (B), TBR (C). Non-glioma patients are depicted as empty circles. The two cases depicted as black dots were considered as outliers (studentized deleted residuals larger than 3) and were excluded from the analysis.

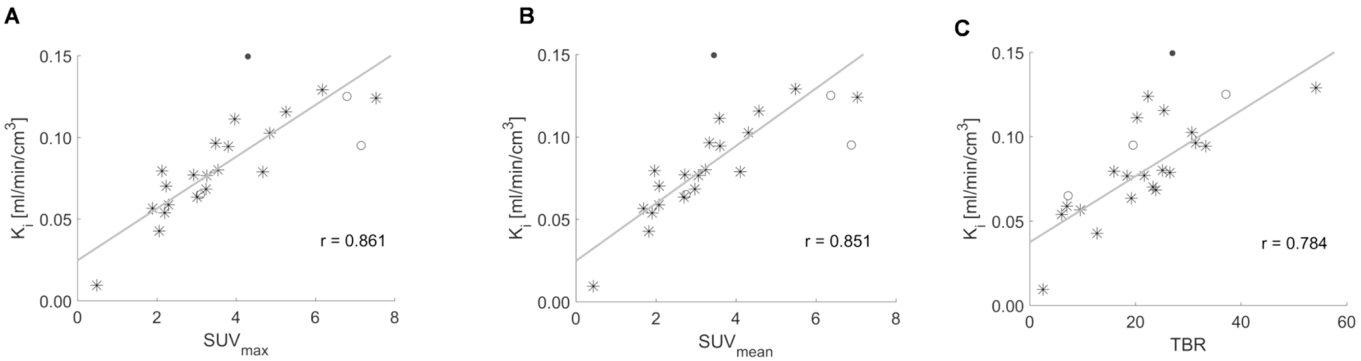

Fig. 6. Correlation between the K_i net influx rate constant and clinical routine measures in the 24 analyzed patients: SUV_{max} (A), SUV_{mean} (B), TBR (C). Non-glioma patients are depicted as empty circles. The patient depicted as a black dot was considered an outlier and excluded from the analysis.

Table 2
Final histopathological diagnosis of the study cohort (n = 24) along with their main kinetic modeling and static parameters from the intratumoral region with highest [^{18}F]F-CHO uptake.

CNS WHO classification (grade)	**N**	**Uptake parameter** (median)				
		Kinetic ‡		*Static*		
		K_1	**K_i**	**SUV_{max}**	**SUV_{mean}**	**TBR**
Glioblastoma, IDHw (grade 4)	**20** *	0.129	0.079	3.37	3.15	22.9
MGMT non-meth	*13*	0.127	0.077	2.93	2.70	19.2
MGMT int-meth	*5*	0.159	0.096	3.55	3.34	25.4
MGMT high-meth	*2*	0.175	0.112	4.99	4.55	43.8
Astrocytoma, IDHm (grade 3) †	**1**	0.017	0.009	0.48	0.43	2.5
CNS-Primary DLBCL	**1**	0.156	0.095	7.16	6.88	19.6
CNS-metastases	**2**	0.202	0.095	4.95	4.56	22.2

* Including 1 patient with gliosarcoma variant and one patient with giant-cell variant. † This astrocytoma IDHm was MGMT non-meth. ‡ Units are ml/min/cm3. N = number of patients; MGMT = O-6-Methylguanine-DNA methyltransferase; int = intermediate; meth = methylation; IDHw = IDH1 wildtype; IDHm = IDH1 mutated; CNS = central nervous system; DLBCL = Diffuse large B-cell lymphoma; TBR = tumor-to-background ratio.

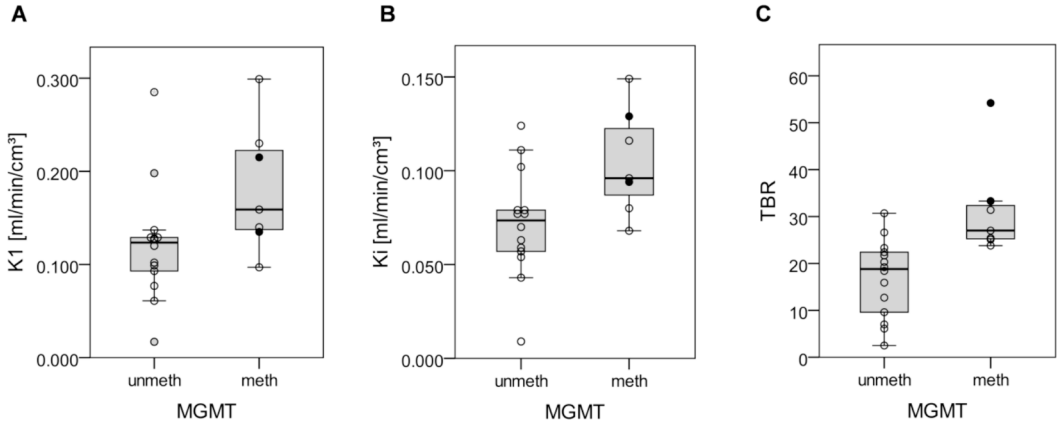

Fig. 7. Box plots and dot plots of K_1 (A), K_i (B) and TBR (C) and their relationship with the MGMT promoter methylation status (unmeth: unmethylated; meth: methylated). The two cases depicted as black dots are those with a high degree of methylation.

parent and metabolized [^{18}F]F-CHO were determined in each patient through a thin-layer-chromatography method, which we described in a previous study (Villar et al., 2019).

The rapid uptake phase followed by a stable activity that was observed in the tumoral curves in our study was in accordance with the dynamic PET acquisitions in HGGs reported by Mertens et al. (Mertens et al., 2012) and Grech-Sollars et al. (Grech-Sollars et al., 2019). The time-activity curves of the three patients with a final diagnosis different from glioma had a similar shape to those of HGGs.

In our cohort, the models that provided the best trade-off between the goodness of fit to the experimental data and the number of free parameters (i.e., with the lowest AIC values) were the 2-tissue-compartment models (2T3k + v_B or 2T4k + v_B). We kept the hypothesis of a trapping or near-trapping mechanism of uptake for [^{18}F]F-CHO for the reasons explained in Section 3.1. The inclusion of the tumoral blood volume fraction v_B in the kinetic model was a requisite to account for the initial vascular peak, as the models failed to represent this early part of the tumoral curve when v_B was set to zero. It is worth noting that the compartmental modeling for [^{18}F]F-CHO has not been subject to a biochemical and kinetic validation in such an extensive way as with other enzyme-mediated trapping radiotracers like [^{18}F]fludeoxyglucose. Nevertheless, there is foregoing preclinical and clinical evidence in several scenarios indicating that the standard and relatively simple 2-tissue or even 1-tissue-compartmental models (Slaets and De Vos, 2013; Verwer et al., 2015; Bolcaen et al., 2016) should be sufficient for the extraction of relevant choline kinetic parameters.

Often in kinetic modeling, it might be the case that different combinations of values of the model parameters can explain a tissue curve equally well, and in these cases we say that the parameters are not identifiable or not reliable. This issue is usually addressed by obtaining the standard error of the parameters from their covariance matrix under certain assumptions. Instead, we favored a more complex approach by

Table 3
Values and performances of [^{18}F]F-CHO uptake parameters to distinguish MGMT methylation status.

Parameter *	**MGMT-m**	**MGMT-nm**	**p-value**	**AUC**	**95 % CI**
K_1	0.159 (0.095)	0.124 (0.042)	0.025	0.806	0.577–0.943
K_i	0.096 (0.049)	0.074 (0.028)	0.020	0.816	0.589–0.949
TBR	27.0 (8.20)	18.8 (13.68)	0.001	0.929	0.728–0.995
SUV_{max}	3.80 (1.77)	2.61 (2.03)	0.046	0.776	0.543–0.926
SUV_{mean}	3.45 (1.34)	2.39 (1.83)	0.046	0.776	0.543–0.926

* Values of the parameters are expressed as median (interquartile range). The units of K_1 and K_i are ml/min/cm^3.
TBR = tumor-to-background ratio; MGMT = O-6-Methylguanine-DNA methyltransferase; MGMT-m = MGMT methylated; MGMT-nm = MGMT non-methylated; AUC = area under the receiver operating characteristic (ROC) curve; 95 % CI = 95 % confidence interval (exact) of the AUC.

simulating models under a realistic experimental noise, which was computed with a Monte Carlo random walk, thus providing a normalized plausible range of values for each parameter as a more intuitive measure of their uncertainty. We concluded that the individual estimates of k_3 and k_2 were not identifiable, which precluded the use of k_3 as an isolated measure of the phosphorylation step. This left K_1 and the influx K_i as the only reliable absolute [^{18}F]F-CHO uptake measures. Some authors have reported k_3 values for [^{18}F]F-CHO in other tumors, generally obtaining poor correlation results with static PET uptake measures or recognizing its low identifiability through percentual standard error (%SE) calculations (Slaets and De Vos, 2013; Grkovski et al., 2020; Bolcaen et al., 2016).

In line with other researchers, we assumed the metabolite [^{18}F]fluorobetaine not to significantly accumulate in tumoral tissue. Yet, before fully accepting our 2-tissue-compartmental model, we confronted it with the more complex but presumably more realistic 3-tissue model with two input functions (3T2i) (Supplemental Fig. 2), taking into account that a damaged BBB could theoretically facilitate [^{18}F]fluorobetaine to pass through (Slaets and De Vos, 2013; Grkovski et al., 2020; Bolcaen et al., 2016). Albeit it is not possible to strictly elucidate whether [^{18}F]fluorobetaine is really internalized or not on the sole basis of our PET macroscopic data, our results support the idea that correcting for [^{18}F]fluorobetaine uptake is not mandatory.

The high complexity of PET kinetic modeling methodology, especially when metabolite corrections are involved, precludes its routine use in the clinics and even the inclusion of a large number of patients in research studies. Hence the interest lies in finding semi-quantitative static measures that adequately reflect the behavior of the more complex dynamic PET parameters. In our cohort of treatment-naive brain tumors, the SUV_{max} at 20–45 min post-injection was the static measure that best correlated with both the net influx K_i and the perfusion-transport rate constant K_1 (Figs. 5 and 6). These results are comparable to those reported by Grkovski et al. (Grkovski et al., 2020) in treated brain metastases and by Utriainen et al. (Utriainen et al., 2003) in their heterogeneous cohort of 12 brain tumors. This supports the idea that the early perfusion and transport steps (K_1) have a probable strong influence on the static uptake measures of [^{18}F]F-CHO. Nevertheless, tumor cell-related features also seem to play a role, since K_i is supposed to partially reflect the choline kinase activity. A correlation analysis between SUV and the phosphorylation rate constant k_3 was not intended due to the lack of identifiability of the latter, as it would have been futile. Thus, the extraction of an absolute quantification [^{18}F]F-CHO uptake parameter purely related to tumor cell biology, as k_3 is intended to be, remains elusive even when applying a full-kinetic modeling methodology.

In our correlation analysis, the behavior of the three non-glioma tumors from our cohort was in line with that of the 21 HGGs. The two cases labeled as outliers (Figs. 5 and 6) were HGGs with unexpectedly high K_1 and K_i values with respect to the corresponding static uptake measures. The reasons for this could not be elucidated, and might be related to an atypical biologic behavior of these HGGs or even to methodological issues.

For methodological and reproducibility reasons, our analysis was limited to the most active PET voxels of the tumors. They turned out to lie inside the MRI gadolinium-enhancing portion of the tumors. A somewhat spatially concordant [^{18}F]F-CHO and gadolinium uptake patterns were indeed expected given the already known influence of BBB disruption in [^{18}F]F-CHO uptake (Herholz, 2017). Nonetheless, some discrepancies were visually observed in eight patients, such as a choline uptake rim peripheral to the gadolinium margins or a mismatch between [^{18}F]F-CHO and gadolinium intensity patterns inside the MRI enhancing margins. Along with the kinetic behavior observed in our PET analysis, we think that this helps to illustrate the fact that [^{18}F]F-CHO uptake is also driven by transport and enzymatic processes related to tumoral cells, apart from the disruption of the BBB.

Lastly, the aforementioned prediction of molecular features in gliomas from the PET-derived parameters was also explored in the present work as a secondary objective. Our analysis was limited to IDH mutation and MGMT promoter methylation, probably the two most relevant biomarkers in HGG. Given that the kinetic analysis was performed over the most active part of the tumor, surgery was also planned in such a way that the part of the tumor with the highest [^{18}F]F-CHO uptake was adequately collected for its in vitro molecular characterization. Moreover, the excellent correlation we subsequently found between the SUV values and influx rate K_i^P at the voxel-level on parametric images (Supplemental Fig. 3) ensured that the hottest spots on the static PET images in the neuronavigation guidance indeed matched to the highest intratumoral influx rate values of [^{18}F]F-CHO. In our cohort essentially composed of glioblastomas IDH wildtype, we found a possible higher tumoral uptake rate of [^{18}F]F-CHO in the presence of methylation of the MGMT gene promoter. This must be considered a merely exploratory result, for which further confirmation is needed with a larger sample size. In the only [^{18}F]F-CHO study to date that has also addressed this issue, Kong et al. (Kong et al., 2021) found no significant association between MGMT methylation status and PET static parameters, including SUV and TBR, in 28 primary diffuse gliomas (CNS WHO grades 2, 3 and 4), a heterogeneous cohort that is not directly comparable to ours. Interestingly, among the studies with other brain PET tracers, Okita et al. found an association between higher uptake of [^{11}C]-methionine and increased MGMT promoter methylation in a cohort of 40 patients with newly diagnosed grade II and III gliomas.

MGMT methylation status is considered as a predictive factor for overall survival in glioblastoma patients treated with alkylating agents (Butler et al., 2020). Nevertheless, as stated by Jacinto and Esteller (Jacinto and Esteller, 2007), MGMT promoter silencing by hypermethylation is a predictive "friend" but at the same time it would indicate an intrinsically more aggressive tumor behavior with an unfavorable natural history if the tumor were left untreated (Komine et al., 2003). In this line, we hypothesize that it would be plausible for MGMT methylated tumors to be statistically associated with a higher metabolic rate, including that of choline and membrane synthesis, as another marker of intrinsic biological aggressiveness in a treatment-naïve scenario.

Finally, we would like to highlight that our patients were recruited between 2016 and 2020 (Fig. 1), hence their histopathological and molecular profiling workup were conducted following the 2016 WHO current recommendations at that time. Thus, the designation of "IDH wildtype" relied on negative R132H-mutant IDH1 immunohistochemistry alone, as sequencing techniques were not readily available at that time. Given that our 20 patients with glioblastoma sufficiently met the requisites for IDH wildtype according to those recommendations, we considered that method appropriate (Louis et al., 2016). Namely, they were older than 54 years (9 patients), or they were 54 years old or younger (11 patients) but without a history of lower-grade glioma and without loss of nuclear ATRX expression (see Supplemental Table). This is a limitation of our study, especially in light of the updated 2021 WHO classification (Louis et al., 2021), which more strongly recommends subsequent IDH1/2 sequencing in younger patients to ensure an accurate classification of glioblastoma as IDH wildtype. Other molecular alterations whose value as prognostic markers has been established in the years following the design of our study could neither be included (Byun and Park, 2022).

5. Conclusions

The tumoral uptake kinetics of [^{18}F]F-CHO in human high-grade gliomas has been described using a complete kinetic modeling methodology, including arterial blood sampling and chromatography-based metabolite corrections. Traditional semi-quantitative SUV-based measures of [^{18}F]F-CHO uptake have been validated against the perfusion-transport (K_1) and the net influx rate (K_i) constants derived from kinetic modeling. These findings provide a rational basis for using PET

static measures in the clinical setting and for further investigating the utility of the widely available radiopharmaceutical [18F]fluorocholine as a quantitative PET biomarker in clinical neuro-oncology.

CRediT authorship contribution statement

Sebastià Rubí: Conceptualization, Formal analysis, Methodology, Investigation, Supervision, Writing – original draft, Writing – review & editing. **Pedro Bibiloni:** Data curation, Formal analysis, Investigation, Methodology, Software, Writing – original draft. **Marina Villar:** Formal analysis, Investigation, Methodology, Writing – original draft. **Marta Brell:** Conceptualization, Supervision, Writing – review & editing. **Manuel Valiente:** Data curation, Formal analysis, Investigation, Methodology. **Margalida Galmés:** Data curation, Formal analysis, Investigation, Methodology. **María Toscano:** Data curation, Formal analysis, Investigation, Methodology. **Gabriel Matheu:** Data curation, Methodology, Supervision, Writing – original draft, Writing – review & editing. **José Luis Chinchilla:** Data curation, Methodology, Software. **Jesús Molina:** Data curation, Methodology, Software. **José Luis Valera:** Methodology, Supervision. **Ángel Ríos:** Data curation, Methodology. **Meritxell López:** Data curation, Methodology. **Cristina Peña:** Resources, Supervision.

Declaration of competing interest

The authors declare that they have no known competing financial interests or personal relationships that could have appeared to influence the work reported in this paper.

Data availability

Data will be made available on request.

Acknowledgements

The authors wish to thank the Interventional Cardiology Department (Hospital Universitari Son Espases, Palma, Spain) and, especially, Dr. Jaume Maristany and Dr. Marcos Pascual for the training provided to S. R. in arterial cannulation. We also thank the help and advice of Prof. Manuel González, Prof. Arnau Mir, Mr. Carlos González and the other members from SCOPIA Research Group of University of the Balearic Islands; Prof. Pablo Aguiar from CIMUS, University of Santiago de Compostela; Dr. Josep Fuster and Dr. Raúl Sánchez from Oncology Department of Hospital Universitari Son Espases (HUSE); Dr. Guillem Frontera, Clinical Pharmacologist and Expert adviser in research methodology from HUSE-IdISBa; and Joan Rebolo from IdISBa's Language Services Department for their language assistance. We would like to give special thanks to Mr. Carlos Enrique, IdISBa Innovation Manager, for their invaluable support and collaboration throughout the project.

Disclosure

This study was financially supported by a project fund from Instituto de Salud Carlos III (Grant ISCIII PI15/01653).

Appendix A. Supplementary data

Supplementary data to this article can be found online at https://doi.org/10.1016/j.nicl.2024.103616.

References

Albert, N.L., Galldiks, N., Ellingson, B.M., van den Bent, M.J., Chang, S.M., Cicone, F., et al., 2024. PET-based response assessment criteria for diffuse gliomas (PET RANO 1.0): a report of the RANO group. Lancet Oncol. 25, e29–e41. https://doi.org/10.1016/S1470-2045(23)00525-9.

Bolcaen, J., Lybaert, K., Moerman, L., Descamps, B., Deblaere, K., Boterberg, T., et al., 2016. Kinetic Modeling and Graphical Analysis of 18F-Fluoromethylcholine (FCho), 18F-Fluoroethyltyrosine (FET) and 18F-Fluorodeoxyglucose (FDG) PET for the discrimination between High-Grade Glioma and Radiation Necrosis in Rats. PLoS One. 11, e0161845 https://doi.org/10.1371/journal.pone.0161845.

Butler, M., Pongor, L., Su, Y.-T., Xi, L., Raffeld, M., Quezado, M., et al., 2020. MGMT Status as a Clinical Biomarker in Glioblastoma. Trends in Cancer. 6, 380–391. https://doi.org/10.1016/j.trecan.2020.02.010.

Byun, Y.H., Park, C.-K., 2022. Classification and Diagnosis of Adult Glioma: A Scoping Review. Brain Neurorehabil. 15 (3), e23 https://doi.org/10.12786/bn.2022.15.e23.

Cuccurullo, V., Di Stasio, G.D., Evangelista, L., Castoria, G., Mansi, L., 2017. Biochemical and Pathophysiological Premises to Positron Emission Tomography With Choline Radiotracers. J. Cell. Physiol. 232, 270–275. https://doi.org/10.1002/jcp.25478.

DeGrado, T.R., Baldwin, S.W., Wang, S., Orr, M.D., Liao, R.P., Friedman, H.S., et al., 2001. Synthesis and evaluation of (18)F-labeled choline analogs as oncologic PET tracers. J. Nucl. Med. 42, 1805–1814.

García Vicente, A.M., Pérez-Beteta, J., Amo-Salas, M., Pena Pardo, F.J., Villena Martín, M., Sandoval Valencia, H., et al., 2019. 18F-Fluorocholine PET/CT in the Prediction of Molecular Subtypes and Prognosis for Gliomas. Clin. Nucl. Med. 44, e548–e558. https://doi.org/10.1097/RLU.0000000000002715.

Grech-Sollars, M., Ordidge, K.L., Vaqas, B., Davies, C., Vaja, V., Honeyfield, L., et al., 2019. Imaging and Tissue Biomarkers of Choline Metabolism in Diffuse Adult Glioma: 18F-Fluoromethylcholine PET/CT, Magnetic Resonance Spectroscopy, and Choline Kinase α. Cancers (basel). 11, 1969. https://doi.org/10.3390/cancers11121969.

Grkovski, M., Kohutek, Z.A., Schöder, H., Brennan, C.W., Tabar, V.S., Gutin, P.H., et al., 2020. 18F-Fluorocholine PET uptake correlates with pathologic evidence of recurrent tumor after stereotactic radiosurgery for brain metastases. Eur. J. Nucl. Med. Mol. Imaging. 47, 1446–1457. https://doi.org/10.1007/s00259-019-04628-6.

Gurrieri, L., De Carlo, E., Gerratana, L., De Maglio, G., Macerelli, M., Pisa, F.E., et al., 2018. MGMT pyrosequencing-based cut-off methylation level and clinical outcome in patients with glioblastoma multiforme. Futur Oncol. 14, 699–707. https://doi.org/10.2217/fon-2017-0437.

Herholz, K., 2017. Brain Tumors: An Update on Clinical PET Research in Gliomas. Semin. Nucl. Med. 47, 5–17. https://doi.org/10.1053/j.semnuclmed.2016.09.004.

Hines, K.E., Middendorf, T.R., Aldrich, R.W., 2014. Determination of parameter identifiability in nonlinear biophysical models: A Bayesian approach. J. Gen. Physiol. 143, 401–416. https://doi.org/10.1085/jgp.201311116.

Jacinto, F.V., Esteller, M., 2007. MGMT hypermethylation: A prognostic foe, a predictive friend. DNA Repair (Amst). 6, 1155–1160. https://doi.org/10.1016/j.dnarep.2007.03.013.

Komine, C., Watanabe, T., Katayama, Y., Yoshino, A., Yokoyama, T., Fukushima, T., 2003. Promoter hypermethylation of the DNA repair gene O6-methylguanine-DNA methyltransferase is an independent predictor of shortened progression free survival in patients with low-grade diffuse astrocytomas. Brain Pathol. 13, 176–184. https://doi.org/10.1111/j.1750-3639.2003.tb00017.x.

Kong, Z., Zhang, Y., Liu, D., Liu, P., Shi, Y., Wang, Y., et al., 2021. Role of traditional CHO PET parameters in distinguishing IDH, TERT and MGMT alterations in primary diffuse gliomas. Ann. Nucl. Med. 35, 493–503. https://doi.org/10.1007/s12149-021-01589-5.

Kong, Z., Jiang, C., Liu, D., Chen, W., Ma, W., Cheng, X., et al., 2021. Quantitative Features From CHO PET Distinguish the WHO Grades of Primary Diffuse Glioma. Clin. Nucl. Med. 46, 103–110. https://doi.org/10.1097/RLU.0000000000003406.

Kwee, S.A., Ko, J.P., Jiang, C.S., Watters, M.R., Coel, M.N., 2007. Solitary brain lesions enhancing at MR imaging: evaluation with fluorine 18 fluorocholine PET. Radiology. 244, 557–565. https://doi.org/10.1148/RADIOL.2442060898.

Lammertsma, A.A., 2017. Forward to the Past: The Case for Quantitative PET Imaging. J. Nucl. Med. 58, 1019–1024. https://doi.org/10.2967/jnumed.116.188029.

Law, I., Albert, N.L., Arbizu, J., Boellaard, R., Drzezga, A., Galldiks, N., et al., 2019. Joint EANM/EANO/RANO practice guidelines/SNMMI procedure standards for imaging of gliomas using PET with radiolabelled amino acids and [18F]FDG: version 1.0. Eur. J. Nucl. Med. Mol. Imaging. 46, 540–557. https://doi.org/10.1007/S00259-018-4207-9.

Louis, D.N., et al., 2016. Gliobastoma, IDH-wildtype. In: Louis, D.N., Ohgaki, H., Wiestler, O.D., Cavenee, W.K. (Eds.), WHO Classification of Tumours of the Central Nervous System (revised 4th Edition). IARC, Lyon, p. 28. ISBN 978-92-832-4492-9.

Louis, D.N., Perry, A., Wesseling, P., Brat, D.J., Cree, I.A., Figarella-Branger, D., et al., 2021. The 2021 WHO Classification of Tumors of the Central Nervous System: a summary. Neuro Oncol. 23, 1231–1251. https://doi.org/10.1093/neuonc/noab106.

Mertens, K., Bolcaen, J., Ham, H., Deblaere, K., Van den Broecke, C., Boterberg, T., et al., 2012. The optimal timing for imaging brain tumours and other brain lesions with 18F-labelled fluoromethylcholine. Nucl. Med. Commun. 33, 954–959. https://doi.org/10.1097/MNM.0b013e328355b6f5.

Pantel, A.R., Viswanath, V., Muzi, M., Doot, R.K., Mankoff, D.A., 2022. Principles of Tracer Kinetic Analysis in Oncology, Part I: Principles and Overview of Methodology. J. Nucl. Med. 63, 342–352. https://doi.org/10.2967/jnumed.121.263518.

Patlak, C.S., Blasberg, R.G., Fenstermacher, J.D., 1983. Graphical Evaluation of Blood-to-Brain Transfer Constants from Multiple-Time Uptake Data. J. Cereb. Blood Flow Metab. 3, 1–7. https://doi.org/10.1038/jcbfm.1983.1.

Roivainen, A., Forsback, S., Grönroos, T., Lehikoinen, P., Kähkönen, M., Sutinen, E., et al., 2000. Blood metabolism of [methyl- 11C]choline; implications for in vivo imaging with positron emission tomography. Eur. J. Nucl. Med. 27, 25–32. https://doi.org/10.1007/PL00006658.

Shrout, P.E., Fleiss, J.L., 1979. Intraclass correlations: Uses in assessing rater reliability. Psychol. Bull. 86, 420–428. https://doi.org/10.1037/0033-2909.86.2.420.

Slaets, D., De Vos, F., 2013. Comparison between kinetic modelling and graphical analysis for the quantification of [18F]fluoromethylcholine uptake in mice. EJNMMI Res. 3, 66. https://doi.org/10.1186/2191-219X-3-66.

Sollini, M., Sghedoni, R., Erba, P.A., Cavuto, S., Froio, A., De Berti, G., et al., 2018. Diagnostic performances of [18F]fluorocholine positron emission tomography in brain tumors. Q. J. Nucl. Med. Mol. Imaging. 62, 209–219. https://doi.org/10.23736/S1824-4785.17.02807-2.

Utriainen, M., Komu, M., Vuorinen, V., Lehikoinen, P., Sonninen, P., Kurki, T., et al., 2003. Evaluation of brain tumor metabolism with [11C]choline PET and 1H-MRS. J. Neurooncol. 62, 329–338. https://doi.org/10.1023/a:1023342516925.

Verwer, E.E., Oprea-Lager, D.E., van den Eertwegh, A.J.M., van Moorselaar, R.J.A., Windhorst, A.D., Schwarte, L.A., et al., 2015. Quantification of 18 F-Fluorocholine Kinetics in Patients with Prostate Cancer. J. Nucl. Med. 56, 365–371. https://doi.org/10.2967/jnumed.114.148007.

Villar, M., Valiente, M., Toscano, M., Galmés, M., González, C., Ortiz, M., et al., 2019. Development of a thin layer chromatography method for plasma correction of [18F] fluorocholine metabolites in positron emission tomography quantification studies in humans. Nucl. Med. Biol. 74–75, 34–40. https://doi.org/10.1016/j.nucmedbio.2019.08.003.